

Demonstration of ROADM Status Visualization Based on Receiver DSP and Digital Twin Modeling

Meng Cai, Xiaomin Liu, Mengfan Fu, Xiaobo Zeng, Yichen Liu, Yihao Zhang, Lilin Yi, Weisheng Hu, and Qunbi Zhuge*

State Key Laboratory of Advanced Optical Communication Systems and Networks, Department of Electronic Engineering, Shanghai Jiao Tong University, Shanghai, China

*Corresponding author: qunbi.zhuge@sjtu.edu.cn

Abstract: We propose a coherent receiver-based telemetry to visualize ROADM status. 100% accuracy of failure localization and 0.67 GHz RMSE of failure estimation are achieved in an 847-km fiber link with 6 WSS nodes. © 2024 The Author(s)

1. Introduction

Reconfigurable optical add-drop multiplexers (ROADMs) based on wavelength selective switches (WSSs) serve as the cornerstone for dynamic signal routing in all-optical networks [1-5]. As network demands for higher capacity and greater flexibility escalate, there has been a surge in deploying large-scale, high-degree ROADM networks [6]. However, this expansion increases the impact of failures in ROADMs, which may cause widespread service disruption across all fibers connected to a ROADM node [7-9]. Therefore, as shown in Fig. 1(a), it is crucial to monitor and visualize the status of all the ROADMs in an optical network. Recent studies have used optical channel monitors (OCMs) at repeater nodes to monitor the soft failure of WSSs due to filter shift (FS) [10]. While effective, the OCM-based solutions incur significant cost overhead. Meanwhile, telemetries based on coherent receiver have been widely investigated since they do not require extra optical devices. However, for WSS filtering effects, the cumulative nature of complex physical effects presents a significant obstacle, complicating a direct correlation between data from the receiver digital signal processing (DSP) and individual ROADM status. To overcome this challenge, artificial neural networks (ANNs) have shown promise in simulations but face challenges in real-world generalization due to the scarcity of actual failure data for training [11]. Another research attempts to monitor fiber loss and FS of optical filters through digital backpropagation [12,13]. However, the method is only validated in a link with 3 fiber spans (150 km) and two optical filter nodes, falling short of practical requirements for long-haul networks which often incorporate more than five ROADM nodes and much longer distances.

In this work, we propose a cost-effective real-time ROADM status visualization telemetry based on receiver DSP and digital twin (DT) modeling, without using additional in-link monitors or historical failure data. In an experimental setup containing an 847-km fiber link with 10 fiber spans and 6 WSS nodes, our telemetry achieves a 100% accuracy in soft failure localization, and a 0.67 GHz root mean square error (RMSE) in failure magnitude estimation, considering both FS and filter tightening (FT) effects. To the best of our knowledge, this is the first demonstration of a coherent receiver-based telemetry that can visualize the status of ROADMs for long-haul networks to support all-optical networking.

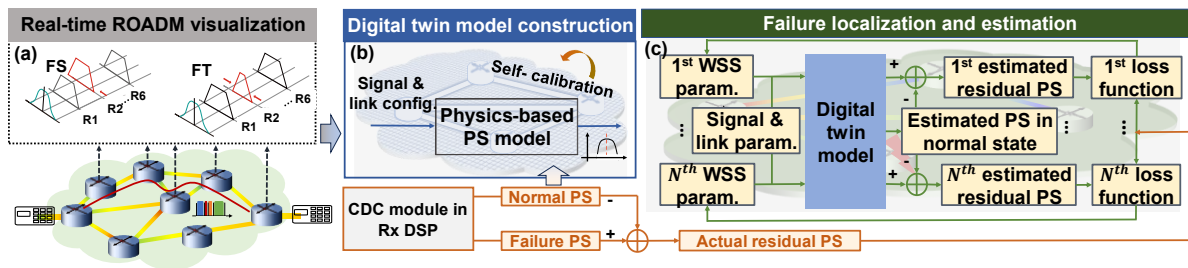


Fig. 1: (a) Real-time ROADM status visualization. The block diagram of the proposed approach: (b) DT model construction; (c) Failure localization and estimation.

2. Principle

The proposed ROADM status visualization telemetry relies on the digital power spectrum (PS) extracted from the receiver DSP and a DT model that can estimate the PS. When the link is in a normal condition, the DT model is aligned with the DSP-monitored PS. When a FS/FT failure occurs in a WSS, a discrepancy arises between the

estimated PS and the actual PS. This discrepancy is exploited to formulate an optimization problem, the solution of which precisely identifies the actual parameters of the failed WSS, thereby achieving real-time ROADM status visualization.

DT Model Construction. The DT model serves as the foundational element of our telemetry, aiming to accurately replicate the PS at the receiver. As shown in Fig. 1(b), the construction of the DT model is a two-stage process. First, we construct a physics-based model as $Y = G^2(f, S) \prod_{i=1}^{W_{num.}} H_i^2(f, W_i) + \sum_{n=1}^{W_{num.}-1} m_n \prod_{i=n+1}^{W_{num.}} H_i^2(f, W_i)$, where $G(f, S)$ represents the pulse shaping function, $H_i(f, W_i)$ is the i^{th} WSS transfer function [2], f denotes the frequency, S is the set of signal parameters, and W_i is the set of the i^{th} WSS parameters. $W_{num.}$ is the number of WSSs, and m_n is the noise power between the i^{th} and $(i + 1)^{th}$ WSS, including the fiber nonlinearity power estimated by the Gaussian Noise (GN) model [14] and the amplified spontaneous emission (ASE) noise power calculated by a numerical model described in [15]. In real systems, the given parameters of the model such as WSS filtering shapes and noise variances are typically inaccurate. To address this issue, we propose a self-calibration stage to construct DT. Based on the DSP-monitored PS in a normal condition, the PS is aligned using a self-learning approach.

Failure Localization and Estimation. When the discrepancy between the DSP-monitored PS and DT-estimated PS is detected, the proposed failure localization and estimation algorithm is activated. The procedure is shown in Fig. 1(c). Since there still exists undesired deviation in initial PS alignment due to factors such as irregular frequency response of transceiver, in our algorithm, we propose to adopt the residual PS by subtracting the PS in the normal state from that of the failure state. An optimization problem focused on WSS parameters is formulated based on the deviation between the DSP-monitored and DT-estimated residual PSs. To solve this optimization problem, we change the parameters of each WSS individually, while keeping the parameters of the other WSSs constant. A loss function is then defined for each WSS, which quantifies the difference between the DT-estimated and DSP-monitored residual PSs. The Broyden–Fletcher–Goldfarb–Shanno (BFGS) algorithm is utilized to minimize these loss functions [16]. Upon examining all WSSs, our algorithm identifies the one corresponding to the minimum value of the loss function as the failed WSS. The optimized parameter of this failed WSS offer insights into the magnitude of the failure, thus enabling real-time ROADM status visualization.

3. Experimental Setup and Results

The experimental setup is depicted in Fig. 2. At the transmitter side, the bit stream is initially mapped into a dual-polarization (DP) quadrature phase shift keying (QPSK) signal, with a symbol rate of 32 Gbaud. The signal is pulse-shaped by a root-raised cosine (RRC) filter with a roll-off factor of 0.1. The transmitted waveforms are generated offline in MATLAB and subsequently uploaded to an arbitrary waveform generator (AWG) with a sampling rate of 120 GSa/s. After being driven by four radio frequency (RF) drivers, the output signal is modulated by a DP-I/Q modulator. The tunable laser's nominal linewidth is 100 kHz, and the central frequency is set to 193.4125 THz. The link incorporates 10 spans of standard single mode fiber (SSMF), cumulatively covering an approximate distance of 847 km. At the end of each span, an erbium-doped fiber amplifier (EDFA) compensates for the fiber loss. Due to the limited experimental environment, only one WSS is utilized to emulate a ROADM node. A programmable filter (Finisar WaveShaper 4000A optical spectrum processor) substitutes for a failed WSS given its tunability in bandwidth and center frequency. This WaveShaper is configured based on a preset WSS transfer function [2]. To compensate for the insertion loss caused by the WSS, an EDFA is employed. At the receiver side, after the IQ errors compensation, frequency offset compensation (FOC) is applied, followed by the chromatic dispersion compensation (CDC) module. Subsequently, an equalizer based on the least mean square (LMS) algorithm is conducted. Finally, carrier phase recovery (CPR) is performed, and the signal-to-noise ratio (SNR) is calculated. To obtain the actual PS, we extract the segmented samples (a 1024 FFT size with a 50% overlap) from the CDC module, compute their PSs, and average the PSs to reduce random noise. The proposed scheme is then conducted.

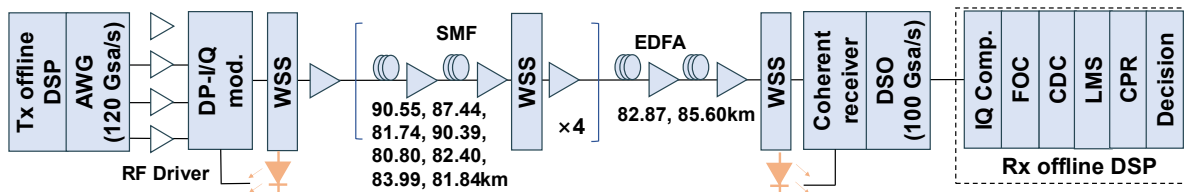


Fig. 2: Experimental setup.

Fig. 3(a) shows the minimized loss function values corresponding to parameter optimization of different WSSs with FS and FT occurred at the fourth WSS. The smallest values are found at the fourth WSS. Fig. 3(b) shows that the

minimum loss function values align closely with actual magnitudes of 10 GHz and 27 GHz for FS and FT, respectively. These results validate our telemetry's capability in failure localization and magnitude estimation. Fig. 3(c) illustrates the rapid convergence of our algorithm, with significant progress after just one iteration. In Fig. 3(d), the error in residual PS significantly decreases after a single iteration, showing the algorithm's effectiveness in aligning WSS parameters.

Then, we evaluate the performance of the telemetry under a wide range of experimental scenarios. The location of the failed WSS varies from 1 to 6, while the launch power varies from 0 dBm to 3 dBm in increments of 1 dB. For FS, at each location and launch power, the deviation value is swept from 5 GHz to 15 GHz and -15 GHz to -5 GHz in increments of 2.5 GHz. For FT, the bandwidth is selected randomly between 19 GHz and 29 GHz, at intervals of 2 GHz. In all cases, the bit error rate (BER) is below the forward-error-correction (FEC) threshold of 0.03. As shown in Fig. 3(e) for FS and (f) for FT, the telemetry localizes the failed filter with a 100% accuracy across the 240 and 144 scenarios for FT and FS, respectively. Fig. 3(g) and (h) show the RMSE, which is 0.67 GHz for both cases. Specifically, 95% of errors for FS are within a range of -1.64 GHz to 0.61 GHz, and for FT, they are between -1.21 GHz and 0.14 GHz. These results demonstrate the high accuracy and adaptability of the proposed telemetry across diverse conditions involving six WSS nodes, and suggest promising scalability to a greater number of WSS nodes. Therefore, with our scheme, it becomes feasible to visualize the status of all ROADMs in an optical network based on coherent receivers.

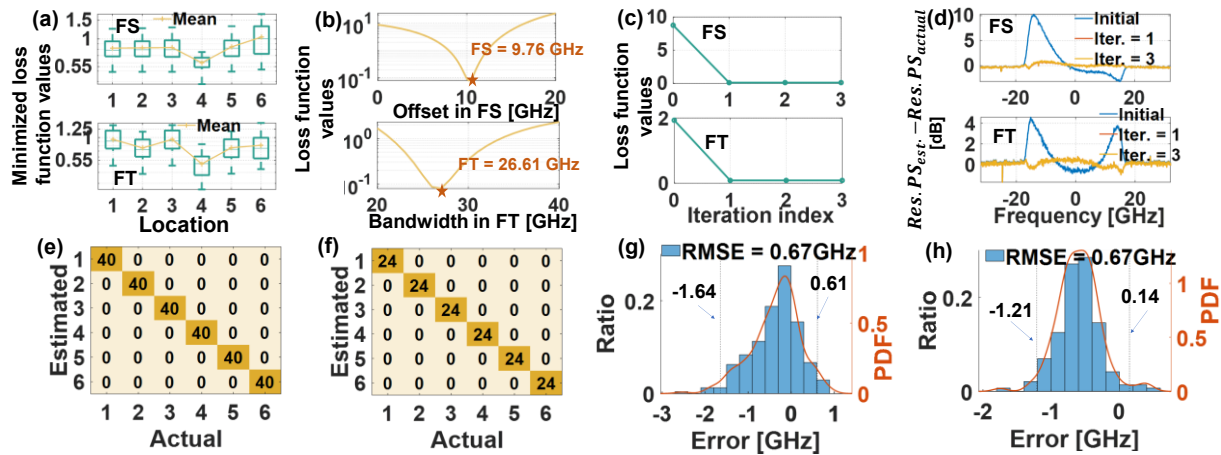


Fig. 3: (a) The minimized loss function values of different WSSs when the fourth WSS fails. (b) The loss function values when the fourth WSS fails with FS = 10 GHz or FT = 27 GHz. (c) The loss function values vs. iteration index. (d) Illustration of errors in residual PS. The confusion matrix for (e) FS and (f) FT. Error histogram for failure magnitude estimation for (g) FS and (h) FT.

4. Conclusions

We propose and demonstrate a coherent receiver-based telemetry that can visualize the status of ROADMs for long-haul networks, without using additional in-link monitors or historical failure data. Our experiments show 100% failure localization accuracy and 0.67 GHz RMSE in failure magnitude estimation. The proposed telemetry will be a key building block for autonomous all-optical networking.

5. Acknowledgements

This work was supported by Shanghai Pilot Program for Basic Research - Shanghai Jiao Tong University (21TQ1400213) and National Natural Science Foundation of China (62175145).

6. References

- [1] S. Gringeri et al., *IEEE Commun. Mag.*, 48, 7, pp. 40-50, 2010.
- [2] C. Pulikkaseril et al., *OE*, vol. 19, no. 9, pp. 8458-8470, 2011.
- [3] S. Oda et al., *JLT*, vol. 35, no. 8, pp. 1350-1356, 2017.
- [4] M. Cai et al., *OE*, vol. 30, no. 14, pp. 24639-24654, 2022.
- [5] Q. Zhuge et al., *JOCN*, vol. 15, no. 8, pp. C242-C262, 2023.
- [6] C. Zhang et al., *IEEE Commun. Mag.*, 57, 4, pp. 138-143, 2019.
- [7] A. P. Vela et al., *JLT*, vol. 35, no. 21, pp. 4595-4604, 2017.
- [8] B. Shariati et al., *JLT*, vol. 37, no. 2, pp. 433-440, 2019.
- [9] H. Lun et al., *JLT*, vol. 41, no. 8, pp. 2312-2322, 2023.
- [10] H. Yamamoto et al., *OFC*, W2A.17, 2023.
- [11] H. Lun et al., *JLT*, vol. 39, no. 9, pp. 2696-2703, 2021.
- [12] T. Tanimura et al., *ECOC*, 1-4, 2019.
- [13] T. Sasai et al., *ECOC*, 1-4, 2020.
- [14] P. Poggiolini, *JLT*, vol. 30, no. 24, pp. 3857-3879, 2012.
- [15] C. R. Giles et al., *JLT*, vol. 9, no. 2, pp. 271-283, 1991.
- [16] J. Nocedal et al., "Numerical optimization.", 1999.